RSC Advances

PAPER

View Article Online
View Journal | View Issue

Cite this: *RSC Adv.*, 2022, **12**, 640

Synthesis, crystal structures and spectroscopic properties of pure YSb_2O_4Br and YSb_2O_4Cl as well as Eu^{3+}- and Tb^{3+}-doped samples†

Ralf J. C. Locke,[a] Felix C. Goerigk,[a] Martin J. Schäfer,[b] Henning A. Höppe[b] and Thomas Schleid *[a]

The quaternary halide-containing yttrium(III) oxidoantimonates(III) YSb_2O_4Cl and YSb_2O_4Br were synthesised through solid-state reactions from the binary components (Y_2O_3, Sb_2O_3 and YX_3, X = Cl and Br) at 750 °C in evacuated fused silica ampoules with eutectic mixtures of NaX and CsX (X = Cl and Br) as fluxing agents. YSb_2O_4Cl crystallizes tetragonally in the non-centrosymmetric space group $P42_12$ with unit-cell parameters of a = 773.56(4) pm and c = 878.91(6) pm, whereas YSb_2O_4Br is monoclinic (space group: $P2_1/c$) with a = 896.54(6) pm, b = 780.23(5) pm, c = 779.61(5) pm and β = 91.398(3)°, both for Z = 4. The two new YSb_2O_4X compounds contain $[YO_8]^{13-}$ polyhedra, which are connected *via* four common edges to form $^2_\infty\left\{\left[YO_{8/2}^{e}\right]^{5-}\right\}$ layers ($d(Y^{3+}–O^{2-})$ = 225–254 pm) without any $Y^{3+}\cdots X^-$ bonds ($d(Y^{3+}\cdots X^-)$ > 400 pm). Moreover, all oxygen atoms belong to ψ^1-tetrahedral $[SbO_3]^{3-}$ units, which are either connected to four-membered rings $[Sb_4O_8]^{4-}$ in the chloride ($Y_2[Sb_4O_8]Cl_2$ for Z = 2) or endless chains in the bromide ($Y_{1/2}(SbO_2)Br_{1/2}$ for Z = 8) by common vertices. With distances of 307 pm in YSb_2O_4Cl and 326 pm in YSb_2O_4Br there are not even substantial bonding $Sb^{3+}\cdots X^-$ (X = Cl and Br) interactions at work. Luminescence spectroscopy on samples doped with trivalent europium and terbium showed an energy transfer from the oxidoantimonate(III) moieties as the sensitizer in the host structure onto the lanthanoid activators.

Received 15th November 2021
Accepted 12th December 2021

DOI: 10.1039/d1ra08382a

rsc.li/rsc-advances

Introduction

In recent years, great attention has been paid to the structural diversity of rare-earth metal(III) oxidoarsenate(III) halides owing to the beneficial inorganic lone-pair antenna at the As^{3+} cations for luminescence applications.[1] Several representatives are known with the formula $RE_5X_3[AsO_3]_4$ (RE = La–Lu, X = F–Br), but all their different crystal structures have the motif of isolated ψ^1-tetrahedral $[AsO_3]^{3-}$ anions in common. The fluoride derivatives (RE = Y, Ho, Tm–Lu)[2,3] crystallize in the tetragonal space group $P4/ncc$ with separated $[AsO_3]^{3-}$ units that form a lone-pair channel along [001], while the chloride derivatives crystallize monoclinically ($C2/c$ for La–Pr,[4–6] $P2/c$ for Nd[5–7] and Sm[2,6]) with a layered structure, in which the $[AsO_3]^{3-}$ units are linked to the chloride layers *via* weak secondary contacts. The three known bromide derivatives (RE = Pr, Sm, Eu)[2] crystallize again in the monoclinic system with space group $P2/c$ and similar coordination features as the chloride derivatives. The motif of ψ^1-tetrahedra $[AsO_3]^{3-}$ is also present in the oxide-halide representatives $RE_3OCl[AsO_3]_2$ and $RE_3OBr[AsO_3]_2$, which crystallize tetragonally in the space groups $P4_2/mnm$ (RE = La)[8,9] or $P4_2nm$ (RE = Ce–Pr, Sm–Dy with X = Cl,[2,4,10] RE = Ce, Nd, Sm, Gd, Tb with X = Br[2]). Like in the $RE_5F_3[AsO_3]_4$ cases (RE = Y, Ho, Tm–Lu), all $RE_3OX[AsO_3]_2$ representatives have a lone-pair tunnel structure of $[AsO_3]^{3-}$ units, but the rare-earth metal–oxygen linkage is different. Furthermore, there are $RE_5O_4Cl[AsO_3]_2$ members (RE = Nd, Pr),[11,12] which crystallize monoclinically in $C2/m$. Not only compounds with isolated $[AsO_3]^{3-}$ anions were synthesised, but also with additional oxidoarsenate(III) units of the pyroanionic species $[As_2O_5]^{4-}$ in the triclinic $RE_3X_2[As_2O_5][AsO_3]$ examples (RE = Sm–Gd with X = Cl,[4,13] RE = Y, Ho–Yb with X = Br[3,13]). These also crystallize in a layered structure (space group: $P\bar{1}$), in which both the $[AsO_3]^{3-}$ and the $[As_2O_5]^{4-}$ anions are bound to the halide layers *via* weak secondary contacts.

The first rare-earth metal(III) oxidobismuthate(III) halide with the composition $Nd_{0.5}Bi_{2.5}O_4Cl$[14] was synthesised by Aurivillius. In this case, the rare-earth metal cation site is mixed with bismuth(III). Only ten years later, $REBi_2O_4Cl$ phases (RE = Y, La, Nd)[15] were the first synthesised representatives without mixed

[a]*Institute of Inorganic Chemistry, University of Stuttgart, Pfaffenwaldring 55, 70569 Stuttgart, Germany*

[b]*Institut für Physik, Augsburg University, Universitätsstraße 1, 86159 Augsburg, Germany*

† Electronic supplementary information (ESI) available. See DOI: 10.1039/d1ra08382a

occupation of the layers. Oppermann *et al.* extended the spectrum of these representatives at first with $ErBi_2O_4I$[16] considerably and found all except the cerium representatives with the composition $REBi_2O_4X$ (RE = La, Pr–Nd, Sm–Lu for X = Cl–I).[16,17] All these representatives crystallize in the tetragonal space group *P*4/*mmm* and form layered structures, in which the rare-earth metal cations are surrounded cube-shaped by eight oxygen atoms $[REO_8]^{13-}$. These cubes are linked to each other *via* common edges. The Bi^{3+} cations form square ψ^1_{ax}-pyramids $[BiO_4]^{5-}$ (ax = axial) with four oxygen, which are linked to each other *via* their corners to form layers as well.

The rare-earth metal(III) oxidoantimonate(III) halides have been neglected in previous research, except for $La_5F_3[SbO_3]_4$,[18] which crystallizes analogously to the $RE_5F_3[AsO_3]_4$ series (RE = Y, Ho, Tm–Lu), and $SmSb_2O_4Cl$[19] postulated by *Oppermann et al.* to be the isotypic light homologue of $SmBi_2O_4Cl$[17] with layers of corner-linked $[SbO_4]^{4-}$ polyhedra (square ψ^1_{ax}-pyramids) with axial lone pairs. It was not until 20 years later that the true composition could be elucidated as $Sm_{1.3}Sb_{1.7}O_4Cl$,[3,20] which crystallizes in principle analogously to the $REBi_2O_4X$ family in the tetragonal space group *P*4/*mmm*. Furthermore, the analogous bromide derivative $Sm_{1.5}Sb_{1.5}O_4Br$[3,20] was discovered, in which there is also a mixed occupation of the antimony position of the Sb^{3+} with Sm^{3+} cations just like in $Sm_{1.3}Sb_{1.7}O_4Cl$. In further studies, the derivatives of the other bromides with RE = Eu–Dy[3,21–23] with the compositions $RESb_2O_4Br$ were discovered. They crystallize in the monoclinic space group $P2_1/c$, but with a different linkage of the antimony–oxygen polyhedra. Here ψ^1-tetrahedral $[SbO_3]^{3-}$ units with only three oxygen atoms are present, which are linked to each other *via* two corners to form chains with the Niggli formula $^1_\infty\{[SbO^v_{2/2}O^t_{1/1}]^-\}$ (v = vertex-sharing, t = terminal), not showing any mixed occupation with RE^{3+} cations. Moreover, the luminescence of trivalent europium and terbium will be investigated and discussed. The oxidoantimonate(III) host structure promises to provide an energy transfer to enhance the luminescence of the 4f–4f activators. Trivalent antimony cations themselves show an efficient 5s–5p excitation that can be used as an antenna for lanthanoid activators[24–26] and antimony(III) compounds have proven to transfer energy previously.[27,28]

Results and discussion

The two rare-earth metal(III) oxidoantimonate(III) halides YSb_2O_4Cl and YSb_2O_4Br were formed from Y_2O_3 and Sb_2O_3 together with YX_3 (X = Cl and Br) as colourless square platelets. YSb_2O_4Cl crystallizes in the tetragonal space group $P42_12$, while YSb_2O_4Br adopts the monoclinic space group $P2_1/c$, just like the already known $RESb_2O_4Br$ representatives with RE = Eu–Dy.[3,21–23] The unit-cell parameters for YSb_2O_4Cl are a = 773.56(4) pm, c = 878.91(6) pm (c/a = 1.136), while a = 896.54(6) pm, b = 780.23(5) pm, c = 779.61(5) pm and β = 91.398(3)° apply for YSb_2O_4Br. The molar volumes of the bromides decrease from $EuSb_2O_4Br$ (V_m = 84.36 cm^3 mol^{-1}) to $DySb_2O_4Br$ (V_m = 82.57 cm^3 mol^{-1}) as consequence of the lanthanoid contraction.[29] Despite being half as heavy the Y^{3+} cation can be classified by its ionic radius between Dy^{3+} and Ho^{3+},[30] which also holds here, indicated with the molar volume of 82.08 cm^3 mol^{-1} for YSb_2O_4Br. The molar volume of YSb_2O_4Cl is with 79.19 cm^3 mol^{-1} considerably smaller as compared to the bromide derivative, due to the lighter and smaller halide anion.

While the monoclinic YSb_2O_4Br shows two crystallographically distinct Y^{3+} positions, the tetragonal YSb_2O_4Cl only comprises one Y^{3+} position. In both cases, however, the Y^{3+} cations are surrounded by eight oxygen atoms that arrange themselves to square hemiprisms $[YO_8]^{13-}$. The $[YO_8]^{13-}$ polyhedra are linked with four of their edges *via* the oxygen atoms to form two-dimensional infinite layers according to the Niggli formula $^2_\infty\{[YO^e_{8/2}]^{5-}\}$ (e = edge-sharing, Fig. 1). These layers run parallel to the (001) plane in YSb_2O_4Cl and to the (100) plane in YSb_2O_4Br. The distances between yttrium and the oxygen atoms range between 227 and 253 pm in YSb_2O_4Cl or

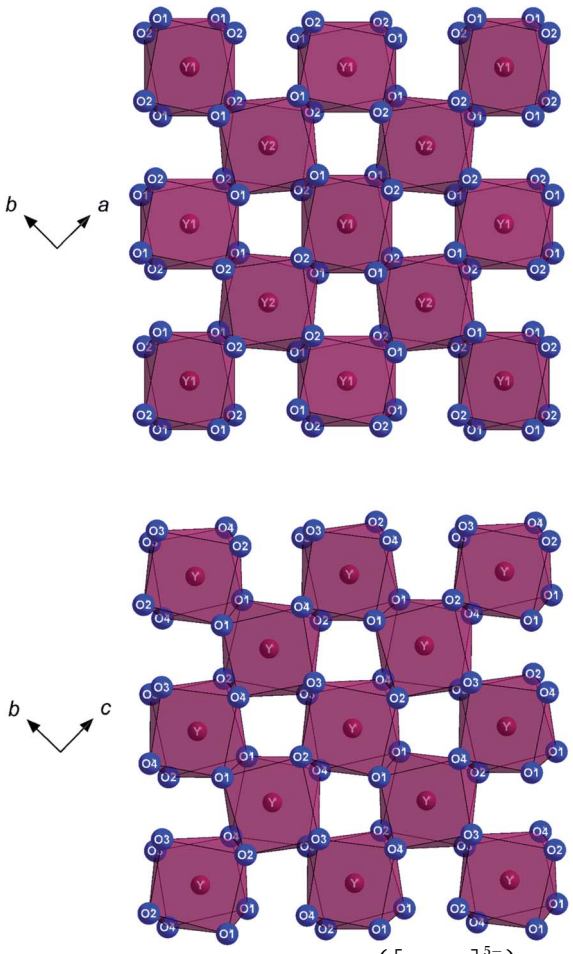

Fig. 1 Two-dimensional infinite layers $^2_\infty\{[YO^e_{8/2}]^{5-}\}$ of edge-linked square hemiprisms $[YO_8]^{13-}$ in the tetragonal crystal structure of YSb_2O_4Cl (top) and in the monoclinic crystal structure of YSb_2O_4Br (bottom).

225 and 253 pm in YSb_2O_4Br. These Y^{3+}–O^{2-} distances are in similar intervals as in yttrium sesquioxide Y_2O_3 ($d(Y^{3+}$–$O^{2-})$ = 225–234 pm) with bixbyite-type structure,[31] where Y^{3+} resides in sixfold oxygen coordination.

The antimony(III) cations occupy one crystallographic position in YSb_2O_4Cl, while there are two different of them in YSb_2O_4Br. Common for both structures, the Sb^{3+} cations form ψ^1-tetrahedral $[SbO_3]^{3-}$ units with three oxygen atoms and the electron lone pair, but this is the only common feature, since in both structures they are linked differently to each other to achieve $\{[SbO_2]^-\}$ motifs. In YSb_2O_4Br, their arrangement is already known from the representatives $RESb_2O_4Br$ (RE = Eu–Dy),[3,21–23] namely the linkage *via* two corners to form one-dimensional infinite chains according to the Niggli formula $^1_\infty\left\{\left[SbO^{\,v}_{2/2}O^{\,t}_{1/1}\right]^-\right\}$ (v = vertex-sharing, t = terminal; Fig. 2). The bridging oxygen atoms show distances of 203–213 pm to the antimony(III) cations and are thus significantly longer than the terminal antimony–oxygen distances of 193–195 pm. Moreover, the terminal O1 atoms of $(Sb1)^{3+}$ exhibit distances to the next $(Sb2)^{3+}$ cation within the chain of $d(Sb2\cdots O1)$ = 317 pm (Fig. 2, red), which is approximately the same as that of the terminal O2 atom of $(Sb2)^{3+}$ to the next $(Sb1)^{3+}$ cation, $d(Sb1\cdots O2)$ = 316 pm, between the chains (Fig. 2, yellow). These meandering chains propagate along [001] and lie parallel within the (100) plane.

The motif of chains occurs more frequently in crystal structures of ternary or quarternary antimony(III)–oxygen compounds. However, Sb^{3+} has than a coordination number of four and forms square ψ^1-pyramids $[SbO_4]^{5-}$ edge-linked according to $^1_\infty\left\{\left[SbO^{\,e}_{2/2}O^{\,'e}_{2/2}\right]^-\right\}$. Examples of representatives for this behaviour are $ASbO_2$ (A = K–Cs),[32,33] $BaSb_2O_4Cl$,[34] $PbSbO_2Cl$[35] and $ZnSbO_2I$.[36] Oxygen antimony chains $^1_\infty\left\{\left[SbO^{\,v}_{2/2}O^{\,t}_{1/1}\right]^-\right\}$ similar as in YSb_2O_4Br can be found in $LiSbO_2$,[37] but here they are twisted to spirals and not planar. In the YSb_2O_4Br structure there are four crystallographic different oxygen atoms, whereas in YSb_2O_4Cl we have only two different ones of them. Unlike the monoclinic compounds YSb_2O_4Br and $RESb_2O_4Br$ (RE = Gd–Dy),[3,21–23] in YSb_2O_4Cl four ψ^1-tetrahedra $[SbO_3]^{3-}$ form a closed ring according to $\{[Sb_4O_8]^{4-}\}$ by vertex-connections (Fig. 3). These rings lie within the (001) plane. The bridging oxygen atoms have distances of 204–210 pm to the Sb^{3+} cations. In contrast, the exo-standing terminal oxygen atoms show significantly shorter contacts of 194 pm just like it is the case for the monoclinic congeners. The terminal oxygen atoms O1 have a distance of $d(Sb\cdots O1)$ = 309 pm to the next non-covalently bonded Sb^{3+} cation, which is a shorter secondary contact than in the monoclinic YSb_2O_4Br representative. Discrete units of antimony and oxygen are relatively rare, but one example would be $Na_3[SbO_3]$,[38] where isolated ψ^1-tetrahedral $[SbO_3]^{3-}$ anions (d(Sb–O) = 189 pm, 3×) are present with their full C_{3v} symmetry. The structural motif of separated $^0_\infty\{[Sb_4O_8]^{4-}\}$ rings is also not novel, but found in valentinite (β-Sb_2O_3).[39] Here they are further connected, not isolated, and show a twisted configuration. The Sb^{3+}–O^{2-} bond lengths in both compounds correspond well with typical antimony–oxygen distances in both crystalline forms of Sb_2O_3 (α:

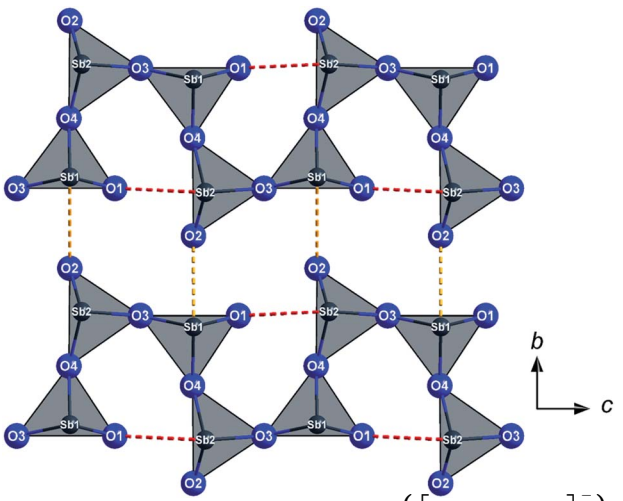

Fig. 2 One-dimensional infinite chains $^1_\infty\left\{\left[SbO^{\,v}_{2/2}O^{\,t}_{1/1}\right]^-\right\}$ of corner-linked ψ^1-tetrahedra $[SbO_3]^{3-}$ in the monoclinic crystal structure of YSb_2O_4Br, which run parallel to the [001] direction. The contacts of the terminal oxygen atoms to the next, not directly bonded Sb^{3+} cations are shown in red within the chains and in yellow between the chains.

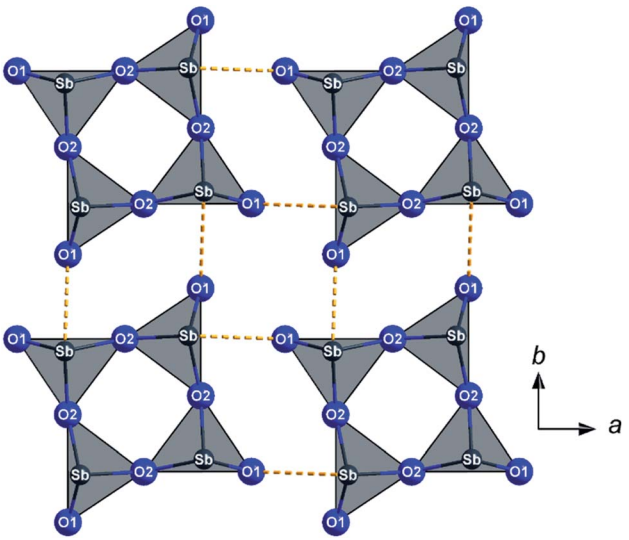

Fig. 3 Isolated rings $[Sb_4O_8]^{4-}$ of four cyclically vertex-linked ψ^1-tetrahedra $[SbO_3]^{3-}$ in the tetragonal crystal structure of YSb_2O_4Cl according to $Y_2[Sb_4O_8]Cl_2$. The contacts of the terminal oxygen atoms to the next, not directly bonded Sb^{3+} cations are shown in yellow.

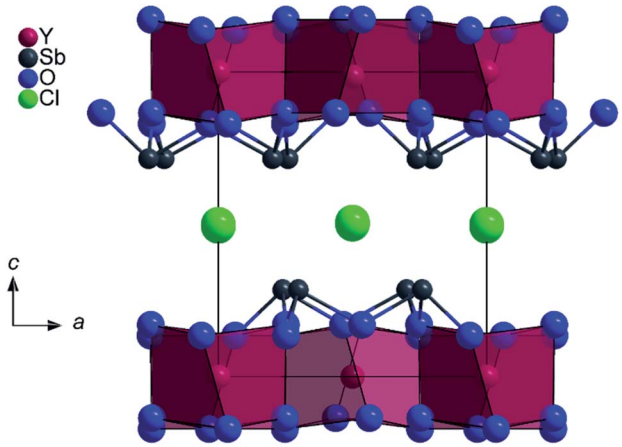

Fig. 4 Extended tetragonal unit cell of YSb_2O_4Cl as viewed along [010].

senarmontite: d(Sb–O) = 198 pm,[40] β: valentinite: d(Sb–O) = 198–202 pm[39]).

In YSb_2O_4Br there is only one crystallographic position for the halide anion, whereas in YSb_2O_4Cl two different ones of them are present. The halide anions show a minimum distance of d(Sb···Cl) = 307 pm to the nearest Sb^{3+} cation in YSb_2O_4Cl and of d(Sb···Br) = 326 pm in YSb_2O_4Br. Their distances to the nearest Y^{3+} cation amount to d(Y···Cl) = 420 pm for YSb_2O_4Cl and d(Y···Br) = 427 pm for YSb_2O_4Br. So at these distances, one can not speak of real coordination in either structure. Between each layer of Sb^{3+} cations there is a layer of halide anions, which in the case of YSb_2O_4Br spreads out parallel to the (100) plane, but parallel to the (001) plane in the case of YSb_2O_4Cl. This halide layer has no contact or connection to any other layer, neither *via* $X^-\cdots Sb^{3+}$ nor *via* $X^-\cdots Y^{3+}$ bonds. However, the layer of Sb^{3+} cations enjoys linkage to the layer of Y^{3+} cations *via* all oxygen atoms according to $^2_\infty\{[YSb_2O_4]^+\}$ in both yttrium(III) oxidoantimonate(III) halides YSb_2O_4X (X = Cl and Br).

Fig. 4 shows an extended unit cell of YSb_2O_4Br with depicted coordination spheres of the Y^{3+} and Sb^{3+} cations. The same applies to Fig. 5, which shows the extended unit cell of YSb_2O_4Cl.

Since the yttrium cations are surrounded by oxidoantimonate layers, an energy transfer from these layers towards any cation doped on the yttrium site could be expected. This was verified *via* luminescence spectroscopy (Fig. 6 and 7), but apparently, the luminescence was quite different for all samples (Fig. 8).

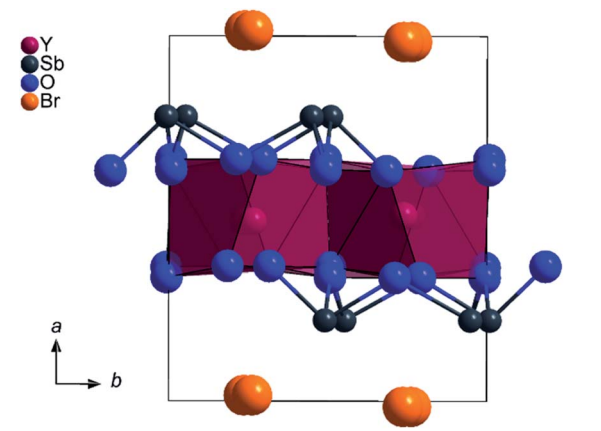

Fig. 5 Extended monoclinic unit cell of YSb_2O_4Br as viewed along [001].

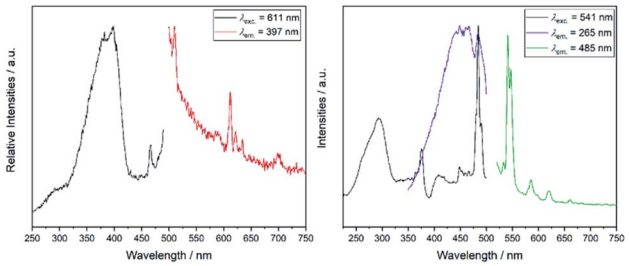

Fig. 6 Fluorescence spectra of YSb_2O_4Cl doped with either Eu^{3+} (left) or Tb^{3+} (right). $\lambda_{exc.}$ describes the wavelength used to record the excitation spectrum, whereas $\lambda_{em.}$ represents the wavelength, at which the emission spectrum was recorded.

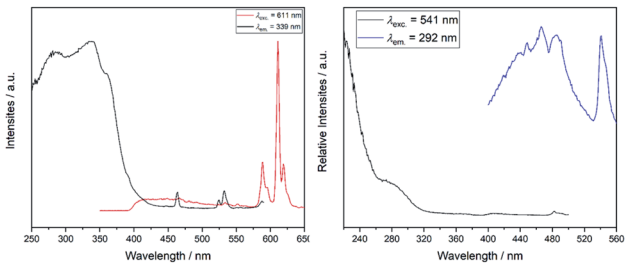

Fig. 7 Luminescence spectra of YSb_2O_4Br doped with either Eu^{3+} (left) or Tb^{3+} (right). $\lambda_{exc.}$ describes the wavelength used to record the excitation spectrum, whereas $\lambda_{em.}$ represents the wavelength, at which the emission spectrum was recorded.

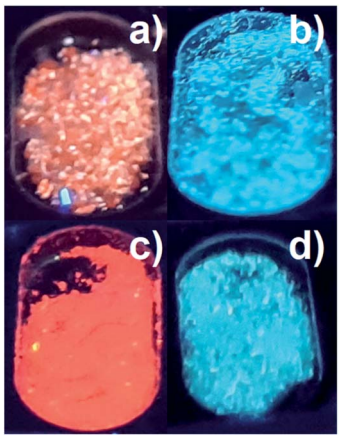

Fig. 8 Comparison of the visible luminescence of the four samples $YSb_2O_4Cl:Eu^{3+}$ (a), $YSb_2O_4Cl:Tb^{3+}$ (b), $YSb_2O_4Br:Eu^{3+}$ (c), and $YSb_2O_4Br:Tb^{3+}$ (d).

$YSb_2O_4Cl:Eu^{3+}$ shows weak, orange-red luminescence. In the spectrum, the weak emission is represented by the low signal-to-noise-ratio. The excitation spectrum is dominated by the broad charge-transfer within the oxidoantimonate host structure peaking at 397 nm. Another band at 467 nm can be attributed to 4f–4f transitions of Eu^{3+}. The emission spectrum features the main emission bands typical for trivalent europium. The band peaking at 612 nm, attributed to the emission $^5D_0 \rightarrow {}^7F_2$, is much more intense than that for $^5D_0 \rightarrow {}^7F_1$, normally located around 595 nm. This supports the experimentally obtained site symmetry of yttrium, as the comparably strong hypersensitive transition is a very good probe for the absence of a local inversion center.

The Tb^{3+}-doped sample of YSb_2O_4Cl shows two different emissions (green and blue) that mix to give a turquoise colour impression. The broad emission in the blue regime with the maximum around 485 nm can be attributed to the emission of the host structure ($^3P_{1,2} \rightarrow {}^1S_0$ transition of the Sb^{3+} lone-pair cation), which has been observed for $LaOBr:Sb^{3+}$ (510 nm)[3] and $GdSb_2O_4Br$ (455 nm)[21] as well as even matches with pure antimony(III) chlorides such as $Cs_2NaSbCl_6$ [41] upon excitation between 255 to 280 nm. Three sharp bands assigned to the 4f–4f transitions $^5D_4 \rightarrow {}^7F_J$ ($J = 3, 4, 5$) were also recorded. The excitation spectrum features two 4f–4f transitions with their respective maxima at 374 and 483 nm. The charge-transfer transition of the host structure is blue-shifted compared to the Eu^{3+}-doped sample and peaks at 294 nm. In both spectra apparently an energy transfer between the host structure and the lanthanoid activator happens upon excitation to enhance the luminescence, but in the Tb^{3+}-doped compound this transfer is obviously incomplete causing a characteristic turquoise emission colour.

The oxidoantimonate bromides show a similar luminescence, when doped with trivalent europium or terbium, but significantly more intense ("heavy-atom effect").[1] $YSb_2O_4Br:Eu^{3+}$ exhibits an excitation spectrum, in which the charge-transfer band of the oxidoantimonate host structure is even more dominating compared to any 4f–4f transition of Eu^{3+}.

It is blue-shifted about 50 nm compared to the chloride. While the same bands were observed as in the oxidoantimonate chloride, their relative intensities are decidedly stronger.

The excitation band around 393 nm, normally the most prominent one, can be only seen as a slight shoulder. In the emission spectrum, the band attributed to the hypersensitive transition $^5D_0 \rightarrow {}^7F_2$ is once again noticeably more intense as compared to the band of the $^5D_0 \rightarrow {}^7F_1$ transition, since the yttrium cation occupies a site without inversion symmetry.

The emission spectrum of $YSb_2O_4Br:Tb^{3+}$ consists of a very broad band, which we assign to the charge-transfer transition of the host structure. The sharp band of the $^5D_4 \rightarrow {}^7F_6$ transition with a maximum around 540 nm is typically the most intense band in Tb^{3+} spectra, the other bands are not observed, due to restrictions on the recorded wavelength regime. Like in the case above, the excitation is blue-shifted and therefore not in the accessible region of the spectrum. Interestingly, the spectrum does not feature either the 4f–5d excitation or any of the typical 4f–4f transitions of Tb^{3+}. This indicates that the Tb^{3+} cations are almost exclusively excited *via* the energy transfer from the oxidoantimonate(III) system ($^1S_0 \rightarrow {}^3P_{1,2}$ transition of the Sb^{3+} lone-pair cation and/or $O^{2-} \rightarrow Sb^{3+}$ charge-transfer excitation).

Table 1 Crystallographic data for YSb_2O_4Cl and YSb_2O_4Br as well as their determination

		YSb_2O_4Cl	YSb_2O_4Br
Crystal system		Tetragonal	Monoclinic
Space group		$P42_12$ (no. 90)	$P2_1/c$ (no. 14)
Lattice constants	a/pm	773.56(4)	896.54(6)
	b/pm	$=a$/pm	780.23(5)
	c/pm	878.91(6)	779.61(5)
	β/°	90	91.398(3)
Formula units, Z		4	4
X-ray density, D_x/g cm^{-3}		5.454	5.803
Molar volume, V_m/cm^3 mol^{-1}		79.185	82.083
Diffractometer		κ-CCD (Bruker-Nonius)	
Wavelength		$\lambda = 71.07$ pm (Mo-K$_\alpha$)	
$F(000)$		760	832
T_{max}/°		27.48	27.39
hkl range ($\pm h_{max}$, $\pm k_{max}$, $\pm l_{max}$)		10, 10, 11	11, 10, 10
Unique reflections		606	1220
Absorption coefficient, μ/mm^{-1}		21.56	27.64
Absorption correction		Program X-SHAPE 2.21 [45]	
R_{int}/R_σ		0.098/0.047	0.132/0.104
R_1/R_1 with $\lvert F_o\rvert \geq 4\sigma(F_o)$		0.049/0.040	0.118/0.060
wR_2/goodness of fit (GooF)		0.085/1.090	0.129/0.986
Structure determination and refinement		Program SHELX-97 [43,44]	
Extinction coefficient, $\varepsilon/10^{-6}$ pm^{-3}		—	0.0008(2)
$\rho_{max/min}/e^-$ 10^{-6} pm^{-3}		1.74/−1.71	2.16/−1.83
Batch scale factor (BASF)[a]		0.45(6)	—
CSD number		2044973	2044975

[a] This value also represents the Flack-x parameter for non-centrosymmetric crystal structures, from which it is transferred into BASF after the TWIN refinement[41–43] as inversion twin.

Table 1 lists the most important crystallographic data for YSb_2O_4Br and YSb_2O_4Cl, while Table 2 gives the atomic coordinates, Wyckoff positions and equivalent isotropic displacement parameters. Table 3 contains selected bond lengths and interatomic distances for YSb_2O_4Cl and YSb_2O_4Br.

Experimental section

Synthesis of YSb_2O_4Cl and YSb_2O_4Br

The yttrium(III) oxoantimonate(III) halides YSb_2O_4X (X = Cl and Br) were synthesised at elevated temperatures *via* solid-state reactions in evacuated silica ampoules (Quarz- und Glasbläserei Müller, Berlin-Adlershof; inner diameter: 10 mm, wall thickness: 1 mm, length: 40 mm). Yttrium oxide (Y_2O_3, ChemPur: 99.9%, 43.57 mg for the chloride, 39.51 mg for the bromide derivative), antimony sesquioxide (Sb_2O_3, ChemPur: 99.9%, 168.75 mg for the chloride, 153.00 mg for the bromide derivative) as well as yttrium chloride (YCl_3, ChemPur: 99.9%, 37.68 mg) and yttrium bromide (YBr_3, Aldrich: 99.9%, 57.49 mg) were used as reactants according to eqn (1). Eutectic mixtures of

Table 2 Atomic coordinates, Wyckoff positions and equivalent isotropic displacement parameters for tetragonal YSb_2O_4Cl (top) and monoclinic YSb_2O_4Br (bottom)

Atom	Wyckoff site	x/a	y/b	z/c	U_{eq}/pm^2
Y1	2a	0	0	0	120(6)
Y2	2c	0	1/2	0.0153(4)	118(6)
Sb	8g	0.24016(8)	0.20182(8)	0.28547(9)	151(2)
O1	8g	0.0629(9)	0.2473(9)	0.1351(11)	165(17)
O2	8g	0.4648(9)	0.2483(9)	0.1705(11)	147(17)
Cl1	2b	0	0	1/2	265(19)
Cl2	2c	0	1/2	0.4929(9)	250(18)
Y	4e	0.4922(2)	0.2368(2)	0.5018(2)	232(5)
Sb1	4e	0.77879(14)	0.05212(15)	0.75550(15)	261(4)
Sb2	4e	0.22116(14)	0.00914(14)	0.79184(15)	240(4)
O1	4e	0.6339(15)	0.0071(13)	0.5739(14)	299(32)
O2	4e	0.3698(14)	0.1843(14)	0.7440(14)	285(29)
O3	4e	0.6613(13)	0.0069(13)	0.9704(13)	212(27)
O4	4e	0.6624(14)	0.2102(13)	0.2595(15)	281(30)
Br	4e	0.0153(2)	0.2371(2)	0.5044(2)	329(5)

sodium chloride (NaCl, Merck: 99.9%, 126 mg) and cesium chloride (CsCl, Aldrich: 99.9%, 674 mg) were used for YSb_2O_4Cl and those of sodium bromide (NaBr, Merck: 99.9%, 203 mg) and cesium bromide (CsBr, ChemPur: 99.9%, 597 mg) for YSb_2O_4Br to improve the reaction speed and the crystal growth as fluxing agents. As doping material europium sesquioxide (Eu_2O_3, ChemPur: 99.9%, 1.7 mg) or terbium chloride ($TbCl_3$, Aldrich: 99.9%, 1.0 mg) were used for YSb_2O_4Cl and europium sesquioxide (Eu_2O_3: ChemPur: 99.9%, 1.5 mg) or terbium bromide ($TbBr_3$, Aldrich: 99.9%, 1.4 mg) for YSb_2O_4Br.

$$Y_2O_3 + YX_3 + 3Sb_2O_3 \xrightarrow{\text{flux}} 3YSb_2O_4X \quad (\text{flux}: \ NaX + CsX, \ X = Cl \text{ and } Br) \tag{1}$$

The reactants were weighed into glassy silica ampoules under inert gas (argon) inside a glove box (Glovebox Systemtechnik, GS Mega E-line), sealed under dynamic vacuum and then subjected to a defined temperature program in a muffle furnace (Nabertherm, L 9/12). This was heated at a rate of 150 K h^{-1} to 750 °C, held there for two days, cooled with 5 K h^{-1} to 666 °C, held for another three days, cooled with 5 K h^{-1} to 530 °C, again held for two days, then cooled with 10 K h^{-1} to 480 °C and finally quenched to room temperature by cutting off the power to the closed furnace. The recovered product samples were washed with 500 ml demineralised water and then dried for 2 h in a drying oven at 120 °C. Under a stereomicroscope, colourless flat, square platelets were visible, clearly larger for YSb_2O_4Cl than for YSb_2O_4Br.

Table 3 Selected interatomic distances (d/pm) for tetragonal YSb_2O_4Cl (left) and monoclinic YSb_2O_4Br (right)

Distance		YSb_2O_4Cl	Distance		YSb_2O_4Br
Y1–O1	(4×)	230.3(10)	Y–O2	(1×)	224.5(12)
Y1–O2	(4×)	247.2(9)	Y–O1	(1×)	226.0(11)
Y2–O1	(4×)	227.3(9)	Y–O1′	(1×)	228.4(12)
Y2–O2	(4×)	253.6(9)	Y–O2	(1×)	234.9(11)
Y1⋯Sb	(4×)	349.06(8)	Y–O4	(1×)	246.6(12)
Y2⋯Sb	(4×)	366.9(2)	Y–O3	(1×)	252.5(11)
Sb–O1	(1×)	193.7(7)	Y–O4′	(1×)	252.7(12)
Sb–O2	(1×)	204.2(7)	Y–O3′	(1×)	252.9(10)
Sb–O2′	(1×)	209.6(7)	Y⋯Sb2	(1×)	351.0(2)
Cl1⋯Y1	(2×)	439.45(3)	Y⋯Sb1	(1×)	351.3(2)
Cl2⋯Y2	(1×)	419.8(9)	Y⋯Sb1′	(1×)	363.9(2)
Cl2⋯Y2′	(1×)	459.1(9)	Y⋯Sb2′	(1×)	367.5(2)
Cl1⋯Sb	(4×)	307.31(7)	Sb1–O1	(1×)	193.0(12)
Cl2⋯Sb	(4×)	320.5(5)	Sb1–O3	(1×)	203.1(10)
Cl2⋯Sb′	(4×)	347.8(4)	Sb1–O4	(1×)	212.9(11)
			Sb2–O2	(1×)	195.1(12)
			Sb2–O4	(1×)	204.9(11)
			Sb2–O3	(1×)	211.3(11)
			Br⋯Y	(1×)	427.6(3)
			Br⋯Y′	(1×)	468.9(3)
			Br⋯Sb1	(1×)	325.8(2)
			Br⋯Sb1′	(1×)	328.1(2)
			Br⋯Sb1″	(1×)	357.6(2)
			Br⋯Sb1‴	(1×)	357.6(2)
			Br⋯Sb2	(1×)	319.7(2)
			Br⋯Sb2′	(1×)	337.5(2)
			Br⋯Sb2″	(1×)	341.9(2)
			Br⋯Sb2‴	(1×)	364.4(2)

Single-crystal X-ray diffraction

Suitable crystals were selected from the samples for single-crystal X-ray diffraction experiments and fixed in glass capillaries (Hilgenberg, Malsfeld; outer diameter: 0.1 mm, wall thickness: 0.01 mm) with grease. The measurements were carried out with a κ-CCD four-circle diffractometer (Bruker-Nonius, Karlsruhe) at room temperature using Mo-K_α radiation. The program package Stoe X-Area 1.86 (2018) was used for data collection and integration. The crystal structures of YSb_2O_4Cl and YSb_2O_4Br were solved in the space groups $P42_12$ and $P2_1/c$, respectively, by direct methods and refined with the SHELX-97 program package.[42–45]

Luminescence spectroscopy

The luminescence spectra of all samples were measured using a Horiba Fluoromax-4 spectrometer scanning from 220 to 800 nm at room temperature. Therefore, finely ground powder samples were filled into the sample holder and subsequently placed in the sample chamber. These measurements were conducted and evaluated with the program FluorEssence.[46] All excitation spectra were corrected to consider the xenon-lamp spectrum.

Conclusions

With YSb_2O_4Br another representative of the known series $RESb_2O_4Br$ (RE = Eu–Dy) could be synthesised and structurally characterised. Thus it also shows the structural motif of ψ^1-tetrahedral $[SbO_3]^{3-}$ groups linked to a meandering chain of the formula $^1_\infty\left\{\left[SbO^{v}_{2/2}O^{t}_{1/1}\right]^-\right\}$ *via* common vertices. As first tetragonal representative of the rare-earth metal(III)

oxoantimonate(III) halides YSb_2O_4Cl (space group: $P42_12$) was obtained. Although its structure shows many similarities to the monoclinic YSb_2O_4Br (space group: $P2_1/c$) representative, it exhibits a different corner-linkage of the ψ^1-tetrahedral $[SbO_3]^{3-}$ units resulting in closed $^0_\infty\{[Sb_4O_8]^{4-}\}$ rings.

The luminescence spectra of samples doped with trivalent europium or terbium confirmed the lack of inversion symmetry around the yttrium cations in both structures, as well as an efficient energy transfer between the oxidoantimonate(III) layers and the lanthanoid(III)-activator cations.

Author contributions

The manuscript was written through contributions of all authors.

Conflicts of interest

There are no conflicts to declare.

Acknowledgements

We thank Dr Falk Lissner and Dr Ingo Hartenbach for the single-crystal X-ray diffraction measurements.

Notes and references

1 G. Blasse and B. C. Grabmaier, *Luminescent Materials*, Springer-Verlag, Berlin, Heidelberg, 1994.
2 F. Ledderboge, Doctoral Dissertation, Univ. Stuttgart, 2016.
3 F. C. Goerigk, Doctoral Dissertation, Univ. Stuttgart, 2021.
4 D.-H. Kang, Doctoral Dissertation, Univ. Stuttgart, 2009.
5 S. Schander, Doctoral Dissertation, Univ. Oldenburg, 2009.
6 F. C. Goerigk, S. Schander, M. Ben Hamida, D.-H. Kang, F. Ledderboge, M. S. Wickleder and T. Schleid, *Z. Naturforsch., B*, 2019, **74**, 497–506.
7 M. Ben Hamida and M. S. Wickleder, *Z. Anorg. Allg. Chem.*, 2006, **632**, 2195–2197.
8 D.-H. Kang, T. Schleid and Z. Anorg, *Allg. Chem.*, 2007, **633**, 1205–1210.
9 H. Ben Yahia, U. C. Rodewald and R. Pöttgen, *Z. Naturforsch., B*, 2010, **65**, 1289–1292.
10 H. Ben Yahia, U. C. Rodewald and R. Pöttgen, *Z. Naturforsch., B*, 2009, **64**, 896–900.
11 H. Ben Yahia, A. Villesuzanne, U. C. Rodewald, T. Schleid and R. Pöttgen, *Z. Naturforsch., B*, 2010, **65**, 549–555.
12 D.-H. Kang, J. Wontcheu and T. Schleid, *Solid State Sci.*, 2009, **11**, 299–304.
13 F. C. Goerigk, S. Schander, M. S. Wickleder and T. Schleid, *Z. Anorg. Allg. Chem.*, 2020, **646**, 985–991.
14 B. Aurivillius, *Chem. Scr.*, 1984, **24**, 125–129.
15 C. J. Milne, P. Lightfoot, J. D. Jorgensen and S. Short, *J. Mater. Chem.*, 1995, **5**, 1419–1421.
16 M. Schmidt and H. Oppermann, *Z. Anorg. Allg. Chem.*, 1999, **625**, 544–546.
17 M. Schmidt, H. Oppermann, C. Henning, R. W. Henn, E. Gmelin and N. Söger, *Z. Anorg. Allg. Chem.*, 2000, **626**, 125–135.
18 A. G. Gukalova and M. N. Tseitlin, *Kristallografiya*, 1988, **33**, 499–501.
19 M. Schmidt, H. Oppermann, M. Zhang-Preße, E. Gmelin, W. Schnelle, N. Söger and M. Binnewies, *Z. Anorg. Allg. Chem.*, 2001, **627**, 2105–2111.
20 F. C. Goerigk and T. Schleid, *Z. Anorg. Allg. Chem.*, 2010, **645**, 1079–1084.
21 F. C. Goerigk, V. Paterlini, K. V. Dorn, A.-V. Mudring and T. Schleid, *Crystals*, 2020, **10**, 1089–1112.
22 R. J. C. Locke, Master Thesis, Univ. Stuttgart, 2021.
23 R. J. C. Locke, F. C. Goerigk and T. Schleid, *Z. Kristallogr.*, 2021, **41**, 78–79.
24 G. Blasse and A. Bril, *J. Chem. Phys.*, 1967, **47**, 1920–1926.
25 E. K. Yukhno, L. A. Bashkirov, P. P. Pershukevich, I. N. Kandidatova, N. Mironova-Ulmane and A. Sarakovskis, *J. Lumin.*, 2017, **182**, 123–129.
26 S. Nigam, V. Sudarsan and R. K. Vatsa, *Opt. Mater.*, 2011, **33**(3), 558–562.
27 A. George, S. Gopi, E. Sreeja, T. Krishnappriya, A. C. Saritha, C. Joseph, N. V. Unnikrishnan and P. R. Biju, *J. Mater. Sci.: Mater. Electron.*, 2020, **31**, 423–434.
28 J. Wang, Y. Cheng, Y. Huang, P. Cai, S. I. Kim and H. J. Seo, *J. Mater. Chem. C*, 2014, **2**, 5559–5569.
29 A. F. Holleman, E. Wiberg and N. Wiberg, *Lehrbuch der Anorganischen Chemie*, Walter-de-Gruyter-Verlag, Berlin, New York, 1985, pp. 91–100.
30 R. D. Shannon, *Acta Crystallogr.*, 1975, **32**, 751–767.
31 M. G. Paton and E. N. Maslen, *Acta Crystallogr.*, 1965, **19**, 307–310.
32 C. Hirschle and C. Röhr, *Z. Anorg. Allg. Chem.*, 2000, **626**, 1305–1312.
33 C. Hirschle and C. Röhr, *Acta Crystallogr.*, 1998, **54**, 1219–1220.
34 F. Thuillier-Chevin, P. Maraine and G. Perez, *Rev. Chim. Miner.*, 1980, **17**, 102–109.
35 L. G. Sillén and L. Melander, *Z. Kristallogr.*, 1941, **103**, 420–430.
36 N. Rück and A. Pfitzner, *Z. Anorg. Allg. Chem.*, 2012, **638**, 1586.
37 B. P. de Laune, R. D. Bayliss and C. Greaves, *Inorg. Chem.*, 2011, **50**, 7880–7885.
38 H. D. Stöver and R. Hoppe, *Z. Anorg. Allg. Chem.*, 1980, **468**, 137–147.
39 B. Antic, P. Oennerud, D. Rodic and R. Tellgren, *Powder Diffr.*, 1993, **8**, 216–220.
40 C. Svensson, *Acta Crystallogr.*, 1975, **31**, 2016–2018.
41 E. W. J. L. Oomen, W. M. A. Smit and G. Blasse, *Chem. Phys. Lett.*, 1987, **138**, 23–28.
42 W. Herrendorf and H. Bärnighausen, *HABITUS: Program for the Optimisation of the Crystal Shape for Numerical Absorption Correction in X-SHAPE, Version 1.06*, Stoe, Darmstadt, 1999, Karlsruhe, 1993, Gießen, 1996.

43 G. M. Sheldrick, *SHELXS-97 and SHELXL-97: Programs for the Solution and Refinement of Crystal Structures from X-Ray Diffraction Data*, Göttingen, 1997.
44 G. M. Sheldrick, *Acta Crystallogr., Sect. A: Found. Crystallogr.*, 2008, **64**, 112–122.
45 M. Weil, *Acta Crystallogr., Sect. E: Crystallogr. Commun.*, 2019, **75**, 26–29.
46 *FluorEssence, Steady State and Frequency Domain Software, Version 3.8.0.60*, HORIBA Scientific, 2008.